Interplay between structural and electronic properties of bundled $Mo_6S_{9-x}I_x$ nanowires

2010 J. Phys.: Condens. Matter 22 505301

(http://iopscience.iop.org/0953-8984/22/50/505301)

IOP Publishing Journal of Physics: Condensed Matter

J. Phys.: Condens. Matter **22** (2010) 505301 (8pp) doi:10.1088/0953-8984/22/50/505301

Interplay between structural and electronic properties of bundled $Mo_6S_{9-x}I_x$ nanowires

Seoung-Hun Kang[1], **Young-Kyun Kwon**[1] **and David Tománek**[2]

[1] Department of Physics and Research Institute for Basic Sciences, Kyung Hee University, Seoul, 130-701, Korea

[2] Department of Physics and Astronomy, Michigan State University, East Lansing, MI 48824-2320, USA

E-mail: ykkwon@khu.ac.kr and tomanek@pa.msu.edu

Received 19 August 2010, in final form 29 October 2010
Published 24 November 2010
Online at stacks.iop.org/JPhysCM/22/505301

Abstract

Using first principles density functional theory, we investigate the structural, electronic and magnetic properties of isolated and bundled $Mo_6S_{9-x}I_x$ nanowires with $x = 3$, 4.5, and 6. The unit cell of each system contains two Mo_6 octahedra decorated with S and I atoms and two S_3 linkages. Due to the bistability of each sulfur linkage, finite-length nanowires or nanowire bundles exhibit many stable structural minima. We explore the structural stability, elastic behavior and electronic structure at all these minima for each composition x. We find that the axial strain and inter-wire interaction in bundles significantly modify the electronic structure. The most intriguing changes occur in nanowires with $x = 4.5$ and 6, which change from metal to semiconductor or undergo a magnetic transition upon axially stretching or compressing the nanowires or upon changing the inter-wire separation.

(Some figures in this article are in colour only in the electronic version)

1. Introduction

Since their discovery almost a decade ago, molybdenum chalcohalide (MCH) nanowires (NWs) [1] have kept puzzling scientists with the complexity of their structure while maintaining their interest owing to a unique combination of properties. The nanowires are extraordinarily stable and often form bundles [2]. Most intriguing are the properties of nanowires with the composition [3] $Mo_6S_{9-x}I_x$, which are air-stable, exhibit a very unusual ability to stretch irreversibly by 30% at very low energy cost [4], have a low shear modulus [5], but a high Young's modulus under specific conditions [6]. These nanowires also exhibit a wide range of electrical transport as well as magnetic properties [7–11].

$Mo_6S_{9-x}I_x$ nanowires have been subject to a wide range of advanced experimental investigations [3, 5, 12–21] to identify their atomic arrangement, with only partial success. Recent structural studies indicate an ordered structure in isolated and bundled $x = 6$ nanowires [16], but a high degree of disorder in the $x = 4.5$ system [22]. Theoretical studies of these complex systems focused on the electronic structure of isolated and bundled nanowires at selected compositions and geometrical arrangements. Selected studies also addressed theoretically the nature of inter-wire interactions and their effect on the electronic structure [8, 10, 12, 16]. Still, a comprehensive study of the equilibrium structure of isolated and bundled $Mo_6S_{9-x}I_x$ nanowires as a function of the axial unit cell length, the inter-wire separation and nanowire orientation for different stoichiometries is missing.

Here we present the results of *ab initio* density functional theory (DFT) calculations for the equilibrium structure, stability and electronic structure of isolated and bundled $Mo_6S_{9-x}I_x$ nanowires. Our study addresses the composition range $0 < x \leqslant 6$ and explores all stable atomic arrangements encountered as a function of the axial unit cell length, the inter-wire separation and nanowire orientation. We report that the inter-wire interaction has an important non-van-der-Waals part that causes significant structural relaxations and bundling energies in excess of 1 eV nm^{-1} wire length. We find that axial strain and inter-wire interaction in bundles modify significantly

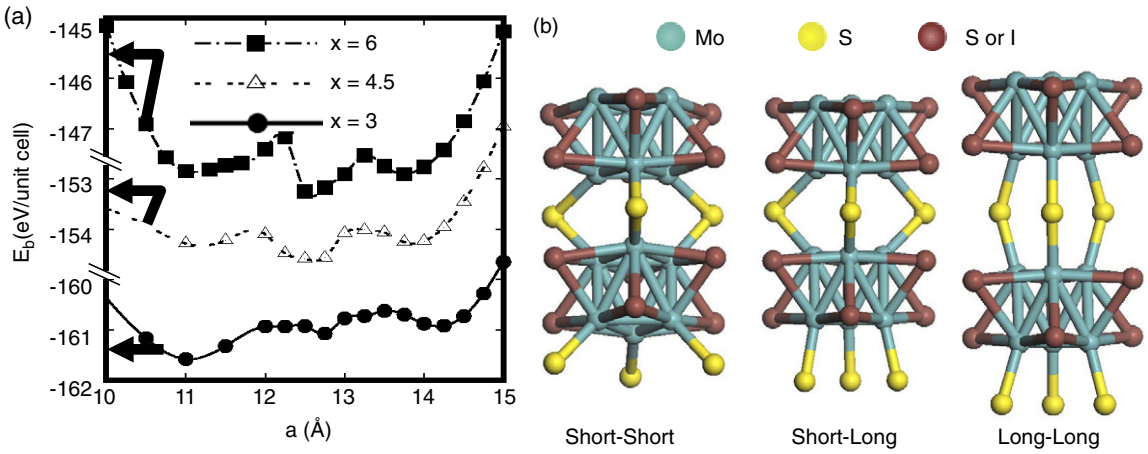

Figure 1. (a) Binding energy per unit cell as a function of the lattice constant a of an isolated $Mo_6S_{9-x}I_x$ nanowire with $x = 3$, 4.5, and 6. For better visualization of the energy differences within each stoichiometry, the energy axis has been split into three segments indicated by an arrow for each binding energy curve. (b) Three stable atomic arrangements in the unit cell of an isolated $Mo_6S_{9-x}I_x$ nanowire corresponding to the three energy minima in (a). The unit cell contains two formula units, each of which contains 6 Mo atoms arranged in an octahedron decorated by six atoms (either S or I atoms) and a S_3 linkage. Due to the bistability of the two S_3 linkages in the unit cell, a nanowire is denoted by 'short–short' representing the structure at the minimum with the shortest a, 'short–long' at the middle minimum, and 'long–long' at the minimum with the longest a.

the electronic structure. The most intriguing changes occur in nanowires with $x = 4.5$ and 6, which change from metal to semiconductor or undergo a magnetic transition upon axially stretching or compressing the nanowires or upon changing the inter-wire separation.

2. Computational method

To investigate the structural, electronic and magnetic properties of isolated and bundled $Mo_6S_{9-x}I_x$ nanowires under different constraints, we carried out *ab initio* DFT calculations using the SIESTA code [23]. We used the Perdew–Zunger form [24] of the Ceperley–Alder exchange–correlation functional [25] in the local density approximation (LDA) to DFT. The behavior of valence electrons was described by norm-conserving Troullier–Martins pseudopotentials [26] with partial core corrections in the Kleinman–Bylander factorized form [27]. An atomic orbital basis with a double-ζ polarization was used to expand the electronic wavefunctions. We complemented the Mo basis by including initially unoccupied 5p orbitals.

Our studies address both infinite isolated nanowires with different stoichiometries and their bundled counterparts. All systems are described by a periodic arrangement of unit cells with axial lattice constant a containing 30 atoms in two formula units of the $Mo_6S_{9-x}I_x$ compound. To describe isolated nanowires in a periodic lattice arrangement, we placed them on a tetragonal lattice with a large inter-wire distance $b = 19.7$ Å, about three times the nanowire diameter, to suppress inter-wire interaction. We sampled the rather short Brillouin zone of these 1D structures with 6 k-points in order to represent adequately the Bloch wavefunctions for the momentum space integration. A $6 \times 6 \times 6$ k-point sampling was used for the densely packed nanowire bundles represented by 3D nanowire arrays. In selected systems the convergence of the electronic structure was tested by a k-point grid which was twice as dense. The charge density and potentials were determined on a real-space grid with a mesh cutoff energy of 150 Ryd, which was sufficient to achieve a total energy convergence of better than 2 meV/atom. We used a confinement energy shift of 0.01 Ryd, which defines the cutoff radii of the atomic orbitals.

All geometries were optimized without any symmetry constraints, by changing the lattice constants a and b as well as atomic positions within the unit cell. We used the conjugate gradient method [28] and relaxed the geometry until the stress on the unit cell vanished in all directions and none of the residual Hellmann–Feynman forces acting on any atom would exceed 1.56×10^{-3} Ryd/a_B, where a_B is the Bohr radius. To probe the possibility of magnetic ordering in the nanostructures, we used the local spin density approximation (LSDA) as a systematic way to estimate the net magnetic moments and the amount of exchange splitting in the nanowires.

3. Results

3.1. Structural properties

The binding energy E_b of an isolated $Mo_6S_{9-x}I_x$ nanowire as a function of the lattice constant a is shown in figure 1(a). The infinite wire is represented by a unit cell containing 30 atoms per two formula units. Each formula unit contains a Mo_6 octahedron with C_3 symmetry decorated with S_{6-x} and I_x atoms, and one S_3 linkage connecting it to a chain structure. The two Mo_6 octahedra in the unit cell are rotated by 180° with respect to each other. We find that S_3 linkages connecting the Mo_6 octahedra are more stable than I_3 linkages [11]. This atomic configuration matches very well the experimental data [16].

The unusual behavior of $E_b(a)$, including three minima, is the consequence of the bistability of the S_3 linkages.

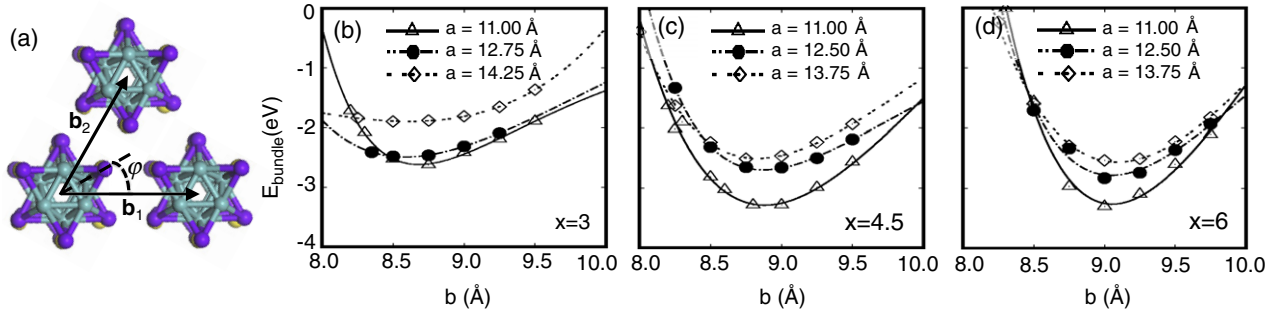

Figure 2. Equilibrium packing of $Mo_6S_{9-x}I_x$ nanowires. (a) End-on view of the structural arrangement of $Mo_6S_{9-x}I_x$ nanowires on a triangular lattice, with inter-wire distance $b = |\mathbf{b}_1| = |\mathbf{b}_2|$. Bundling energy E_{bundle} as a function of b at three equilibrium axial lattice constants a, for (b) $Mo_6S_6I_3$, (c) $Mo_6S_{4.5}I_{4.5}$, and (d) $Mo_6S_3I_6$. The bundling energy is the difference between the binding energies E_b per formula unit of isolated and bundled nanowires.

Mo–S–Mo bonds in S_3 linkages form preferentially either an acute (short linkage) or an obtuse angle (long linkage) [9]. With two such linkages per unit cell, we can distinguish a 'short–short' from a 'short–long'/'long–short' and a 'long–long' configuration, as shown in figure 1(b). Whereas transitions between these structural optima require little energy investment, the elastic constant associated with further stretching the 'long–long' isomer is very high [11], in agreement with experimental data [5]. As we show in this paper, the specific configuration of the S_3 linkages within the unit cell plays a key role in determining not only the total energy, but also the electronic structure of the nanowires.

To explore the equilibrium geometries of a $Mo_6S_{9-x}I_x$ nanowire, in particular the effect of the S_3 linkages, we globally optimized the structure of $x = 3$, 4.5, 6 nanowires while constraining the value of the axial lattice constant a. The results for the calculated binding energy $E_b(a)$ with respect to isolated atoms are shown in figure 1(a) for the different compositions. To make sure that the structure at a given value of a is a global and not a local optimum, we started our optimization procedure by subjecting uniformly expanded or compressed nanowires to random distortions, or using geometries based on semi-empirical force fields. We considered a structure to represent the optimum geometry when the same structural arrangement was achieved starting from different geometries. As seen in figure 1(a), independent of composition, all isolated nanowires exhibit three geometrical optima. For $x = 3$ we find $a_{\text{eq}} = 11.00$, 12.75, and 14.25, and for $x = 4.5$ and 6 we find $a_{\text{eq}} = 11.00$, 12.50, and 13.75 Å. The binding energy per unit cell decreases gradually with increasing iodine concentration.

The existence of several energy minima in $E_b(a)$ is explained by the bistability of two S_3 linkages in the unit cell. Figure 1(b) shows three stable atomic arrangements corresponding to three optima, which we call the 'short–short', 'short–long' and 'long–long' S_3 linkage configurations. For each composition, the three (meta-) stable configurations have a similar binding energy and are separated by relatively low energy barriers of about 1 eV/unit cell. This implies the possibility to transform one structure to another by stretching or compressing, like in a linear ratchet, at moderate forces accessible in atomic force microscopy (AFM) [4].

Earlier theoretical studies report weak inter-wire interaction in $Mo_6S_{9-x}I_x$ nanowire bundles [8, 12, 16], but many experimental studies observed stable bundled structures [3, 5, 12, 13, 15–21]. This discrepancy would be due to calculations done at a fixed inter-wire distance without geometrical relaxation. We therefore studied the structural properties of bundled $Mo_6S_{9-x}I_x$ nanowires at all three stable axial unit cell sizes a and different inter-wire distances for each composition.

The geometry of a nanowire bundle, represented by a periodic array of $Mo_6S_{9-x}I_x$ nanowires on a triangular lattice spanned by lattice vectors $\mathbf{b}_1$ and $\mathbf{b}_2$, is shown in figure 2(a). To get an unbiased insight into the potential energy surface of nanowire bundles, we investigated unit cells with a range of lattice constants a and b near the expected optimum and subsequently globally optimized the structure of $x = 3$, 4.5, 6 nanowires while constraining a and b. To separate the large cohesive energy of a nanowire from the much smaller inter-wire interactions in the total energy, we defined the bundling energy E_{bundle} as the difference between the binding energies E_b per formula unit of isolated and bundled nanowires.

Our results for $E_{\text{bundle}}(b)$ at the different compositions x and equilibrium values of the axial lattice constant a, shown in figures 2(b)–(d), indicate the degree of bundle stabilization due to the attractive inter-wire interaction. These results indicate that the equilibrium inter-wire distance b_{eq} depends most sensitively on the composition x and much less on the length of the axial lattice constant. The equilibrium inter-wire distances b for the 'short–short', 'short–long' and 'long–long' configuration, are 8.59 Å $\lesssim b_{\text{eq}} \lesssim$ 8.68 Å for $x = 3$, 8.83 Å $\lesssim b_{\text{eq}} \lesssim$ 8.87 Å for $x = 4.5$, and 9.02 Å $\lesssim b_{\text{eq}} \lesssim$ 9.09 Å for $x = 6$. Iodine-richer bundles exhibit a larger equilibrium inter-wire distance since the atomic radius of iodine is larger than that of sulfur.

Our results in figure 2 indicate that the bundling energy depends on the axial unit cell size a and the composition x, and generally ranges from 1.9 eV $\lesssim |E_{\text{bundle}}| \lesssim$ 3.3 eV/unit cell, corresponding to $\lesssim$0.1 eV/atom. This relatively large value of E_{bundle} suggests that $Mo_6S_{9-x}I_x$ nanowires form stable bundled structures that may be hard to separate. We find that the most stable bundles are formed at the smallest values of the axial lattice constant a, corresponding to the 'short–short' structure,

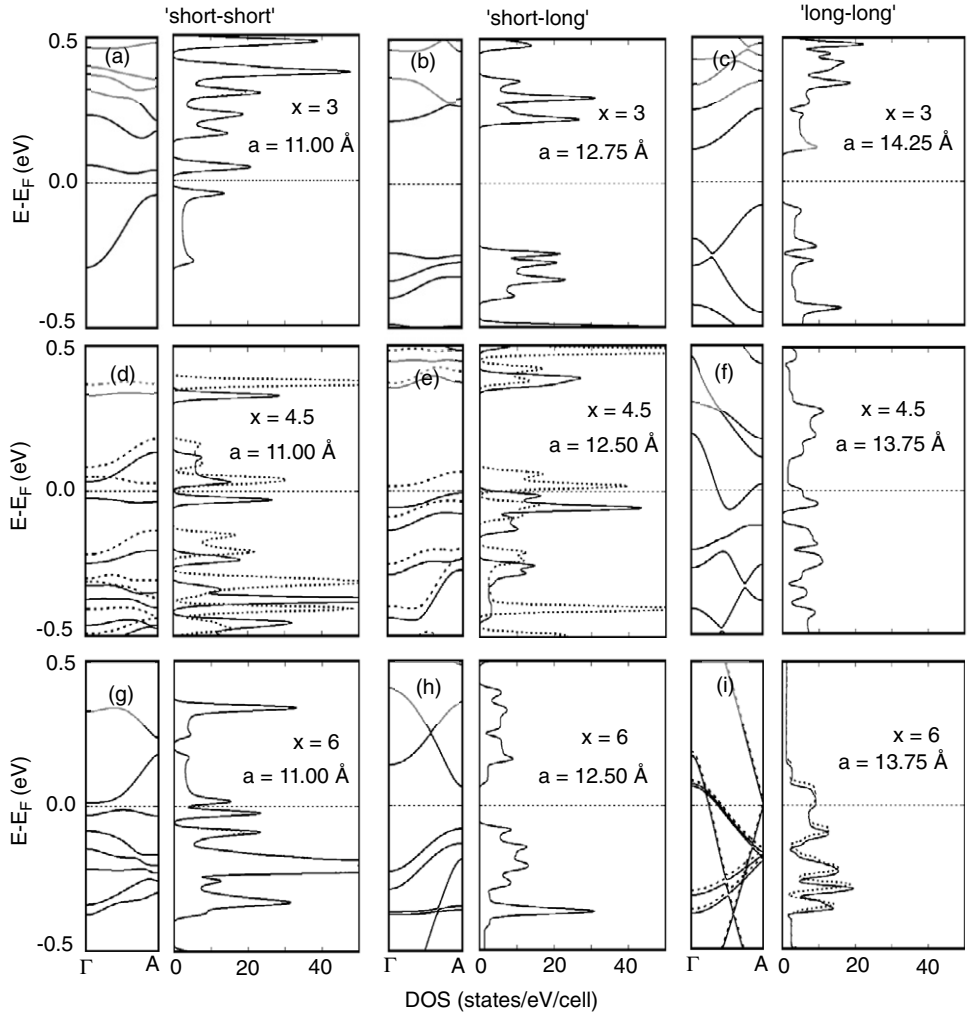

Figure 3. Electronic band structure $E(k)$ along the axial direction Γ–A and the corresponding density of states (DOS) of isolated $Mo_6S_{9-x}I_x$ nanowires at three equilibrium lattice constants a corresponding to three $E_b(a)$ optima in figure 1(a) for (a)–(c) $Mo_6S_6I_3$ ($a = 11.00$, 12.75, and 14.25 Å), (d)–(f) $Mo_6S_{4.5}I_{4.5}$ ($a = 11.00$, 12.5, and 13.75 Å), and (g)–(i) $Mo_6S_3I_6$ ($a = 11.00$, 12.50, and 13.75 Å). Results for 'short–short', 'short–long' and 'long–long' configurations are displayed in columns. The densities of states have been convoluted with 0.02 eV wide Gaussians.

for all compositions. The systems with the shortest axial unit cell also represent the stiffest structures. We find a tendency to bundle and for the axial stiffness to decrease gradually from the 'short–short' to the 'long–long' configuration. Also, we find a uniform increase of the bundling energy with increasing iodine concentration x.

3.2. Electronic structure

The potential application of $Mo_6S_{9-x}I_x$ nanowires as building blocks in nano-electronics depends crucially on their electronic structure. The presence of S_3 groups in the system is very favorable, since sulfur is well known to form an ideal contact to Au lead material [9, 11]. In the following we describe the electronic structure at the different stable geometries, discussed in section 3.1. We discuss the results for isolated nanowires in figure 3 and for ordered nanowire arrays in figures 4 and 5 for the different compositions. A comprehensive summary of our results is presented in table 1.

We present results for the electronic band structure $E(k)$ as well as the density of states (DOS) of isolated $Mo_6S_{9-x}I_x$ nanowires with $x = 3$, 4.5, 6 at the three stable axial unit cell sizes a_{eq} in figure 3. Results in the same column, corresponding to the same structural minimum, indicate no simple trends in the electronic band structure near the Fermi level with changing iodine concentration. We conclude that the changing orbital hybridization, which causes structural relaxations, plays a crucial role.

As seen in figures 3(a)–(c), isolated $Mo_6S_{9-x}I_x$ nanowires with $x = 3$ are semiconducting at all structural optima. The fundamental gap in the isolated nanowire with $x = 6$ at the 'short–short' configuration, seen in the band structure in figure 3(g) is very narrow and nearly suppressed by the convolution used in the DOS. As seen in figure 3(h), the fundamental gap opens upon stretching the structure to the 'short–long' configuration. We observe a closing of the gap and the occurrence of a magnetic instability in the metallic system with the 'long–long' configuration, depicted in figure 3(i).

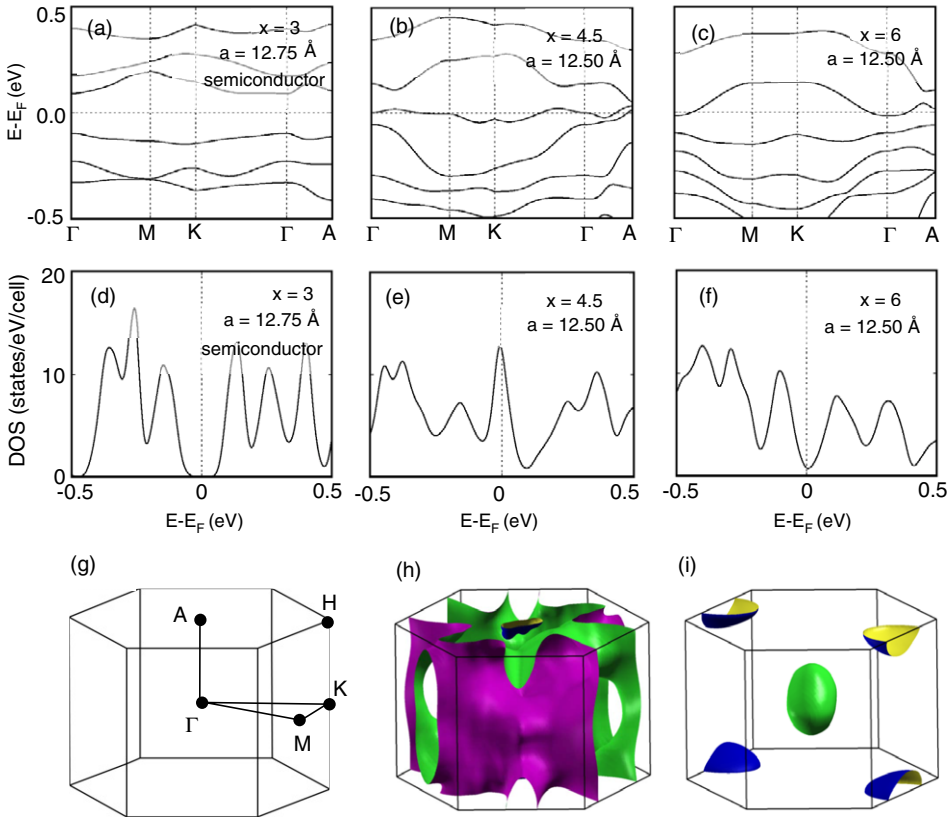

Figure 4. (a)–(c) Electronic band structure $E(k)$, (d)–(f) the corresponding density of states (DOS) and (g)–(i) the Fermi surface of bundled $Mo_6S_{9-x}I_x$ nanowires at the lattice constant a corresponding to the 'short–long' configuration depicted in figure 1(b). Results for $x = 3$ at $a = 12.75$ Å and $x = 4.5, 6$ at $a = 12.50$ Å are displayed in columns. The densities of states have been convoluted with 0.02 eV wide Gaussians. Since $Mo_6S_6I_3$ is a semiconductor and does not have a Fermi surface, we depict the empty Brillouin zone and the high-symmetry points in (g).

Table 1. Dependence of electronic properties of isolated and bundled $Mo_6S_{9-x}I_x$ nanowires on their composition x, axial equilibrium length a_{eq}, and equilibrium inter-wire distance b_{eq}. We use sc for semiconducting, met for metallic, mag for magnetic, and non-mag for non-magnetic.

x	a_{eq} (Å)	b_{eq} (Å)	Isolated wire	Bundle
3	11.00	8.68	sc	sc
	12.75	8.59	sc	sc
	14.25	8.61	sc	sc
4.5	11.00	8.85	sc, mag[a]	met, non-mag
	12.50	8.87	sc, mag[a]	met, non-mag
	13.75	8.83	met, non-mag	met, non-mag
6	11.00	9.06	sc	met, non-mag
	12.50	9.02	sc	met, non-mag
	13.75	9.09	met, mag	met, mag

[a] Exchange splitting opens up a narrow gap at E_F.

The 'short–short' configuration of the $Mo_6S_{4.5}I_{4.5}$ nanowire exhibits a flat band at E_F and gives rise to a sharp peak in the density of states. The results of our LSDA calculations, shown in figure 3(d), indicate the occurrence of a magnetic instability [9] that turns the nanowire into a semiconductor with a 75 meV gap at E_F and a net magnetic moment of 1.0 μ_B/unit cell. Even though ferromagnetic ordering should not persist in these 1D systems at finite temperatures, we may still expect the occurrence of magnetism in finite segments of $Mo_6S_{4.5}I_{4.5}$. According to figure 3(e), the $x = 4.5$ system with the 'short–long' configuration undergoes a similar magnetic instability, turning it into a narrow-gap magnetic semiconductor with the same magnetic moment of 1.0 μ_B/unit cell. We found a very sensitive dependence of the band dispersion at E_F on the precise atomic positions in the unit cell, causing the occurrence or disappearance of magnetism upon very small atomic displacements at room temperature. Only in the 'long–long' configuration does the $Mo_6S_{4.5}I_{4.5}$ nanowire turn metallic and non-magnetic, as seen in figure 3(f).

To better understand the effect of bundle formation on the electronic structure, we displayed the band structure, density of states and Fermi surface of $Mo_6S_{9-x}I_x$ nanowire arrays with $x = 3, 4.5, 6$ in figure 4 in the 'short–long' and in figure 5 in the 'long–long' configuration. As we discuss in the following, some of these results differ significantly from the data obtained for the 'short–short' configuration [29]. In the absence of any inter-wire interaction, we would expect all bands to be flat along the Γ–M–K–Γ path in the Brillouin zone shown in figures 4(g) and 5(g). Also, in this case, the Γ–A band dispersion along the wire axis should be equal to that in figure 3

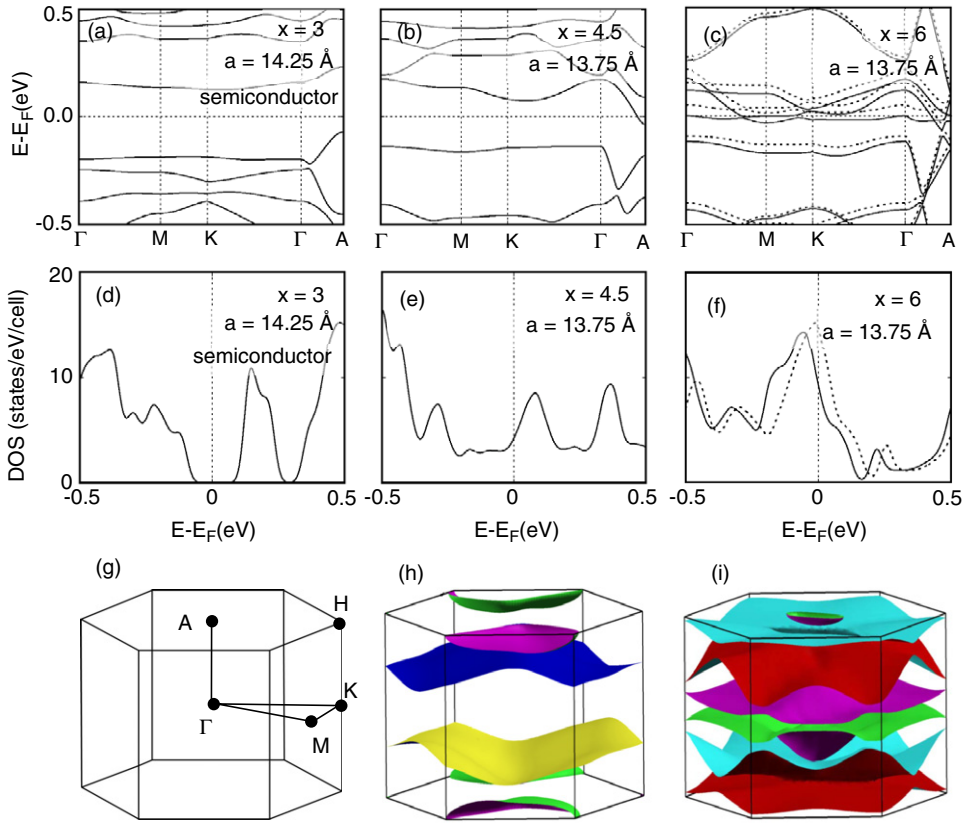

Figure 5. (a)–(c) Electronic band structure $E(k)$, (d)–(f) the corresponding density of states (DOS) and (g)–(i) the Fermi surface of bundled $Mo_6S_{9-x}I_x$ nanowires with the lattice constant a corresponding to the 'long–long' configuration depicted in figure 1(b). Results for $x = 3$ at $a = 14.25$ Å and $x = 4.5$, 6 at $a = 13.75$ Å are displayed in columns. As indicated in (c) and (f), the $Mo_6S_3I_6$ nanowire array is ferromagnetic; the Fermi surface in (i) corresponds to the 'spin-up' configuration. The densities of states have been convoluted with 0.02 eV wide Gaussians. Since $Mo_6S_6I_3$ is a semiconductor and does not have a Fermi surface, we depict the empty Brillouin zone and the high-symmetry points in (g).

for isolated nanowires. This is clearly not the case, as seen in the band structures displayed in figures 4(a)–(c) and 5 (a)–(c), reflecting the influence of the inter-wire interaction discussed earlier.

According to figure 3 and table 1, all isolated $Mo_6S_{9-x}I_x$ nanowires investigated here are semiconductors, with the exception of the $Mo_6S_{4.5}I_{4.5}$ and the $Mo_6S_3I_6$ nanowire in the 'long–long' configuration at $a = 13.75$ Å. This changes significantly due to the modified band dispersion in bundles. The band structure displayed in figures 4(a)–(c) for the 'short–long' and in figures 5 (a)–(c) for the 'long–long' configuration indicates that only the $x = 3$ nanowires remain semiconducting when forming bundles and the other systems turn metallic. In spite of the flat band reflected in a peak at E_F in the DOS of $Mo_6S_{4.5}I_{4.5}$, shown in figures 4(b) and (e), this system remains non-magnetic in the 'short–long' configuration at $a = 12.50$ Å. A different scenario emerges in the iodine-richer $Mo_6S_3I_6$ nanowire in the 'long–long' configuration at $a = 13.75$ Å, a peak in the DOS at E_F, seen in figure 5(f), is sufficiently high to cause a magnetic instability without opening a gap.

We found it interesting that trends in the bundling energy for the different compositions and axial unit cell optima, shown in figures 2(b)–(d), are reflected also in the band structures shown in figures 4(a)–(c) for the 'short–long' and figures 5(a)–(c) for the 'long–long' configuration. The inter-wire interaction in bundles is reflected in the band dispersion in the Γ–M–K–Γ plane that is normal to the wire axis. Since we find the bundling energy to decrease with increasing a in figure 2, so does the band dispersion decrease with increasing a when comparing results in figures 4 and 5 for the same composition. Comparing trends across equivalent values of a_{eq}, the increase in the bundling energy with increasing iodine concentration in figure 2 is reflected in an increased band dispersion normal to the wire axis in figures 4(a)–(c) and figures 5(a)–(c). Since the smallest bundling energy occurs in the 'long–long' configuration, the Γ–A band dispersion along the wire axis in that configuration most closely resembles that in the isolated wires, depicted in figures 3(c), (f) and (i).

The largest difference in the electronic structure between the 'short–long' and the 'long–long' configuration occurs in the shapes of the Fermi surfaces, shown in figures 4(h), (i), 5(h) and (i) for the metallic systems. Even though the Fermi surface of the $x = 4.5$ system spreads across the entire Brillouin zone independent of a, its shape changes from a set of warped planes parallel to the wire axis at $a = 12.50$ Å, shown in figure 4(h), to a set of warped planes normal to the wire axis at $a = 13.75$ Å, shown in figure 5(h). As mentioned

above, the latter system more closely resembles the behavior of non-interacting nanowires, in which case there should be no dispersion in the Γ–M–K–Γ plane.

We observe even larger changes in the Fermi surface of the $x = 6$ system as a function of the axial lattice constant. There changes primarily reflect the transformation from a bad metal with a low DOS at E_F in figure 4(c) to a good metal with a high DOS in figure 5(c). Our results for the Fermi surface of the bad metal at $a = 12.50$ Å, shown in figure 4(i), indicate an isolated electron pocket near Γ and isolated hole pockets near the Brillouin zone boundary. Very different and richer is the Fermi surface of the good metal at $a = 13.75$ Å. Since this metallic system is magnetic, there are two separate Fermi surfaces associated with the majority and minority spin. We show in figure 5(i) only the Fermi surface associated with the majority spin, as it resembles closely the minority spin surface. The Fermi surface is distributed throughout the Brillouin zone; we expect the conductance of the corresponding nanowire bundles to be large and nearly isotropic.

One of the initial motivations of this study was to understand better why the $Mo_6S_{4.5}I_{4.5}$ system appears structurally much more disordered than the $Mo_6S_3I_6$ system [16, 22]. For one, the decoration pattern of the Mo_6 octahedra by iodine atoms only is unique in the $x = 6$ nanowire, whereas several decoration patterns with a similar total energy are possible in the $x = 4.5$ system [11]. In practice we may expect a distribution of several patterns along each nanowire with $x = 4.5$. This structural disorder would also likely cause significant changes in the local inter-wire separation and electronic structure.

There are two more reasons to expect deviations in the electronic structure of a realistic system from our results for ordered crystalline arrays. Since the inter-wire interaction potential in figure 2 is relatively soft, we may expect fluctuations of the inter-wire separation within the bundles, which in turn affect the hybridization of orbitals on adjacent nanowires and thus the electronic structure. Finally, there is the possibility of torsion in isolated and bundled nanowires in analogy to free and bundled carbon nanotubes [30]. The torsion mode is expected to be very soft due to the flexibility of the S_3 linkages. Whereas a small amplitude torsion should not affect the electronic structure of isolated nanowires, it may do so in bundles. On the one hand, the inter-wire interaction in nanowire bundles has been reported to be rather isotropic in a previous study [29] of the bundling energy as a function of the nanowire orientation angle φ, defined in figure 2(a). In view of this fact, we expect nanowires not to be perfectly straight, but rather twisted to some small degree in realistic bundles. Even though the total energy may be independent of φ, changes in the inter-wire hybridization at changing orientations are expected to modify the electronic structure with respect to the idealized geometry discussed in this work.

4. Summary and conclusions

We investigated the structural, electronic and magnetic properties of isolated and bundled $Mo_6S_{9-x}I_x$ nanowires with $x = 3$, 4.5, and 6 using first principles density functional calculations. The unit cell of each system contains two Mo_6 octahedra decorated with S and I atoms and two S_3 linkages. Due to the bistability of each sulfur linkage, finite-length nanowires or nanowire bundles exhibit many stable structural minima. We explored the structural stability, elastic behavior and electronic structure at all these minima for each composition x. We found that the axial strain and inter-wire interaction in bundles significantly modify the electronic structure. The most intriguing changes occurred in nanowires with $x = 4.5$ and 6, which changed from metal to semiconductor or underwent a magnetic transition upon axially stretching or compressing the nanowires or upon changing the inter-wire separation.

Acknowledgments

We thank Sora Park and Teng Yang for useful discussions. DT was supported by the National Science Foundation Cooperative Agreement #EEC-0832785, titled 'NSEC: Center for High-rate Nanomanufacturing'. YK was partly supported by the NRF of Korea grant KRF-2010-0015656.

References

[1] Remskar M, Mrzel A, Skraba Z, Jesih A, Ceh M, Demsar J, Stadelman P, Levy F and Mihailovic D 2001 *Science* **292** 479–81
[2] Kis A, Mihailovic D, Remskar M, Mrzel A, Jesih A, Piwonski I, Kulik A J, Benoit W and Forro L 2003 *Adv. Mater.* **15** 733–6
[3] Vrbanić D *et al* 2004 *Nanotechnology* **15** 635
[4] Hassanien A, Tokumoto M, Mrzel A, Mihailovic D and Kataura H 2005 *Physica* E **29** 684–8
[5] Kis A, Csanyi G, Vrbanic D, Mrzel A, Mihailovic D, Kulik A and Forro L 2007 *Small* **3** 1544–8
[6] Mihailovic D 2009 *Prog. Mater. Sci.* **54** 309–50
[7] Bercic B, Pirnat U, Kusar P, Dvorsek D, Mihailovic D, Vengust D and Podobnik B 2006 *Appl. Phys. Lett.* **88** 173103
[8] Vilfan I and Mihailovic D 2006 *Phys. Rev.* B **74** 235411
[9] Yang T, Okano S, Berber S and Tomanek D 2006 *Phys. Rev. Lett.* **96** 125502
[10] Popov I, Yang T, Berber S, Seifert G and Tomanek D 2007 *Phys. Rev. Lett.* **99** 085503
[11] Yang T, Berber S and Tomanek D 2008 *Phys. Rev.* B **77** 165426
[12] Meden A, Kodre A, Gomilsek J, Arcon I, Vilfan I, Vrbanic D, Mrzel A and Mihailovic D 2005 *Nanotechnology* **16** 1578–83
[13] Uplaznik M, Bercic B, Strle J, Ploscaru M I, Dvorsek D, Kusar P, Devetak M, Vengust D, Podobnik B and Mihailovic D 2006 *Nanotechnology* **17** 5142–6
[14] Paglia G, Bozin E, Vengust D, Mihailovic D and Billinge S 2006 *Chem. Mater.* **18** 100–6
[15] Dassenoy F, Joly-Pottuz L, Martin J M, Vrbanic D, Mrzel A, Mihailovic D, Vogel W and Montagnac G 2007 *J. Eur. Ceram. Soc.* **27** 915–9
[16] Nicolosi V *et al* 2007 *Adv. Mater.* **19** 543–7
[17] Vrbanic D, Meden A, Novosel B, Pejovnik S, Umek P, Ponikvar M and Mihailovic D 2007 *J. Nanosci. Nanotechnol.* **7** 982–5
[18] Mandrino D, Vrbanic D, Jenko M, Mihailovic D and Pejovnik S 2008 *Surf. Interface Anal.* **40** 1289–93

[19] Rangus M, Remskar M and Mrzel A 2008 *Microelectron. J.* **39** 475–7
[20] Andzane J, Prikulis J, Dvorsek D, Mihailovic D and Erts D 2010 *Nanotechnology* **21** 125706
[21] Hummelgård M, Zhang R, Carlberg T, Vengust D, Dvorsek D, Mihailovic D and Olin H 2010 *Nanotechnology* **21** 165704
[22] Nicolosi V 2009 private communication
[23] Soler J M, Artacho E, Gale J D, García A, Junquera J, Ordejón P and Sánchez-Portal D 2002 *J. Phys.: Condens. Matter* **14** 2745–79
[24] Perdew J P and Zunger A 1981 *Phys. Rev.* B **23** 5048
[25] Ceperley D M and Alder B J 1980 *Phys. Rev. Lett.* **45** 566
[26] Troullier N and Martins J L 1991 *Phys. Rev.* B **43** 1993
[27] Kleinman L and Bylander D M 1982 *Phys. Rev. Lett.* **48** 1425
[28] Hestenes M R and Stiefel E 1952 *J. Res. Natl Bur. Stand.* **49** 409–36
[29] Kang S H, Kwon Y K and Tománek D 2010 *Phys. Rev.* B **82** 205427
[30] Kwon Y K and Tomanek D 2000 *Phys. Rev. Lett.* **84** 1483–6